Molecular Architecture and Rheological Characterization of Novel Intramolecularly Crosslinked Polystyrene Nanoparticles

ANISH TUTEJA,[1] MICHAEL E. MACKAY,[1] CRAIG J. HAWKER,[2,3] BROOKE VAN HORN,[3]* DEREK L. HO[4]

[1]Department of Chemical Engineering and Materials Science, Michigan State University, East Lansing, Michigan 48824

[2]Materials Research Laboratory, University of California, Santa Barbara, California 93106

[3]IBM Almaden Research Center, San Jose, California 95120

[4]National Institute of Standards and Technology, Gaithersburg, Maryland 20899

Received 12 September 2005; revised 21 February 2006; accepted 24 March 2006
DOI: 10.1002/polb.20826
Published online in Wiley InterScience (www.interscience.wiley.com).

ABSTRACT: Novel polystyrene nanoparticles were synthesized by the controlled intramolecular crosslinking of linear polymer chains to produce well-defined single-molecule nanoparticles of varying molecular mass, corresponding directly to the original linear precursor chain. These nanoparticles are ideal to study the relaxation dynamics/processes of high molecular mass polymer melts, as the high degree of intramolecular crosslinking potentially inhibits entanglements. Both the nanoparticles and their linear analogs were characterized by measuring their intrinsic viscosity, hydrodynamic radius (R_h), and radius of gyration (R_g). The ratio R_g/R_h was computed to characterize the molecular architecture of the nanoparticles in solution, revealing a shift toward the constant density sphere limit with increasing crosslink density and molecular mass. Further, confirming particulate behavior, Kratky plots obtained from neutron scattering data show a shift toward particle-like nature. The rheological behavior of the particles was found to be strongly dependent on both the extent of intramolecular crosslinking and molecular mass, with a minimal viscosity change at low crosslinking levels and a gel-like behavior evident for a large degree of crosslinking. These and other results suggest the presence of a secondary mode of polymer relaxation/movement besides reptation, which in this case, is influenced by the total number of crosslinked loops present in the nanoparticle. ©2006 Wiley Periodicals, Inc. J Polym Sci Part B: Polym Phys 44: 1930–1947, 2006

INTRODUCTION

There has been a phenomenal growth of interest in the development and study of nanomaterials because of the many unusual and unique effects that can be seen only in this size range. Nanoparticles serve the role of being an important building block for the production of nanomaterials with a broad range of future and present applications in electronic, mechanical, and biomedical processes.[1]

Various polymer particles with size ranging from 50 nm to several microns are now commercially available; however, the synthesis and study

Correspondence to: M. E. Mackay (E-mail: mackay@msu.edu)
*Present address: Washington University in St. Louis, St. Louis, MO.

Journal of Polymer Science: Part B: Polymer Physics, Vol. 44, 1930–1947 (2006)

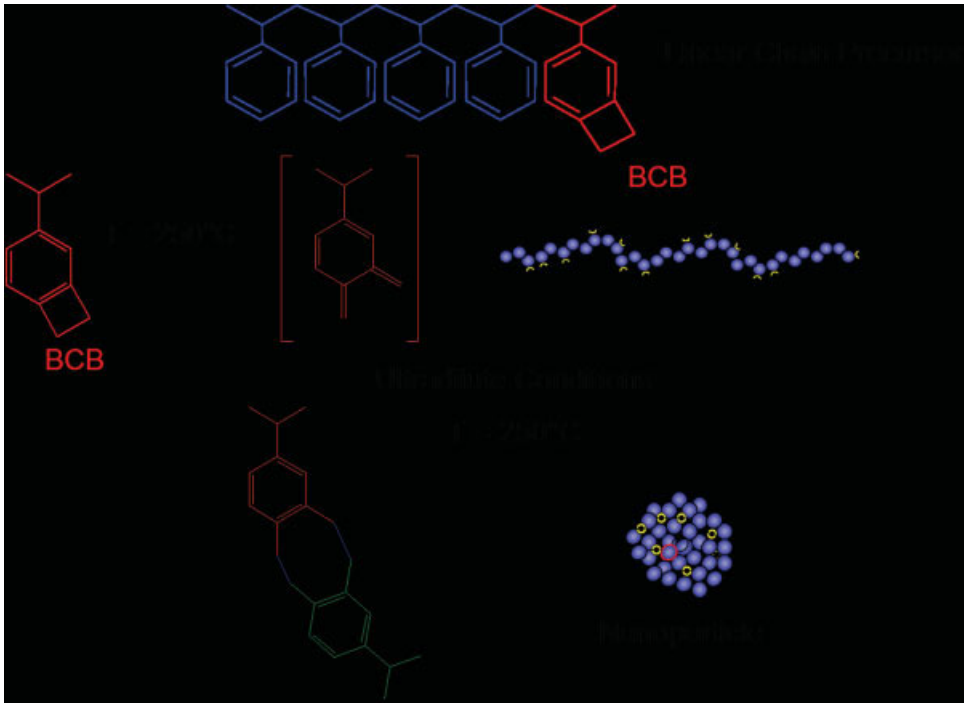

Figure 1. Schematic representation of the intramolecular crosslinking process.

of smaller polymeric nanoparticles still remains a challenge. In this work, we characterize unimolecular, organic (polystyrene) nanoparticles produced by the intramolecular crosslinking of functional polymers, having sizes ranging from 3 to 15 nm. These molecules are then used to discern the various modes of relaxation in both low and high molecular mass polymers as a function of crosslink density.

The synthesis[2] of the nanoparticles was accomplished by first incorporating the crosslinking agent 4-vinylbenzocyclobutene (denoted as BCB in Fig. 1) into the linear polystyrene chain as a comonomer, and subsequently collapsing the chain under ultradilute conditions by intramolecular crosslinking. The extent of crosslinking within the nanoparticles produced by this method can therefore be controlled by the amount of crosslinker that is copolymerized within the linear polymer.

Considerable work has been done previously to initiate intramolecular crosslinking within polymers and then to measure the effects of this crosslinking on the polymer properties in solution. Kuhn and Balmer[3] carried out crosslinking in an aqueous solution of poly(vinyl alcohol) by the addition of terephthaldehyde, and then studied the intrinsic viscosity behavior of the crosslinked polymer as a function of increasing solution concentration of the starting monomer. They found that when the monomer concentration was low, the intrinsic viscosity of the solution decreased, indicating a decrease in polymer size because of intramolecular crosslinking; however, at higher monomer concentrations the intrinsic viscosity increased, indicating intermolecular crosslinking. Also, Longi and Rossi[4] synthesized intramolecularly crosslinked styrene–methyl acrylate copolymers and found that the intrinsic viscosity decreased in proportion to the number of crosslinks per polymer.

Research in this area was furthered by Martin and Eichinger[5,6] who conducted the first complete theoretical and experimental analysis to determine the change in the unperturbed radius of gyration ($R_{g0}(\theta)$) of a linear coil caused by intramolecular crosslinking. First, they developed a method to determine $R_{g0}(\theta)$ by assuming that the crosslinked polymer consists of a number of subpolymer Gaussian chains. Eichinger[7] had found earlier that $R_{g0}(\theta)$ for any Gaussian chain can be computed by finding its Kirchoff matrix and its generalized inverse. Thus, the unperturbed dimensions of the whole molecule could be computed, as the sum of its parts. Using this analysis, for an intramolecularly

crosslinked polymer chain, the Zimm–Stockmayer contraction factor (g) is given as

$$g = 1 - 0.7\ \rho_x^{0.5} \quad (1)$$

where g is the ratio of $R_{g0}(\theta)^2$ for the crosslinked molecule to that of the equivalent linear chain and ρ_x is the crosslink density defined as the moles of crosslinks per mole of Gaussian statistical segments.

To confirm their theoretical analysis, they produced intramolecularly crosslinked polystyrene using a Friedel–Crafts crosslinking reaction, with (dichloromethyl)benzene as the crosslinking agent. The change in the molecules' hydrodynamic radii (R_h), caused by the crosslinking, was then experimentally measured by means of photon correlation spectroscopy (dynamic light scattering; DLS). The results were related to the Zimm–Stockmayer contraction factor by the relation

$$h = \sqrt{g} \quad (2)$$

where h is the ratio of $R_{h0}(\theta)$ for the crosslinked particle to that for the linear chain and $R_{h0}(\theta)$ is the unperturbed hydrodynamic radius. Indeed they found close agreement between the observed unperturbed dimensions of the crosslinked molecules and their theoretical predictions.

Our systems differ from theirs primarily due to the extent of intramolecular crosslinking induced in polystyrene. The most heavily crosslinked polystyrene used by Martin and Eichinger had 100 crosslinks per molecule which amounts to 1 in every 48 monomer units on average being crosslinked (mention of a more tightly crosslinked sample is given in a table, yet, no data are presented on this system). In contrast, even the lightly crosslinked polystyrene synthesized in this study has 1 in 40 monomer units on average crosslinked, whereas the more tightly crosslinked molecule has 1 in every 5 monomer units crosslinked.

At this point it is important to mention the significant work done by Antonietti et al. in the development and rheological characterization of intramolecularly crosslinked polystyrene microgels. Apart from detailing the clever techniques employed by the authors to synthesize and characterize the microgels,[8–11] their work also provides a descriptive introduction to the rheological behavior of intramolecularly crosslinked particles.[12,13] Comparison between these studies and the present work is however reserved for the results and discussion section and next we provide a brief introduction to the mechanism of chain motion in polymer melts.

The terminal viscosity of polymer melts is a strong function of the polymer molecular mass (M). Below the so-called critical mass for *entanglement coupling*[14] (M_c) the viscosity scales as M^1 while above M_c a much larger power law, ~3.4–3.8 power,[15–17] is present. This steep increase of viscosity above M_c is attributed to the presence of entanglements, which are basically constraints on the motion of polymer chains caused by the fact that the chains cannot pass through each other. Such a geometrically constrained environment thus limits molecular motion/diffusion of the chain to a snake-like motion along its own contour,[18] denoted as reptation.[19]

The reptation model has been very useful in providing a mechanistic understanding of bulk polymer dynamics, as well as in providing a quantitative explanation of the plateau modulus, diffusion coefficient, and scaling of viscosity with molecular mass (in its native form the theory predicts a power law as 3 instead of 3.4). However, results from many computer simulations and experiments[20] on widely differing systems (for example ring polymers,[21] star polymers,[22,23] crosslinked microgels,[12] block copolymers,[24] and polymer blends[25–27]) do not match reptation predictions, clearly demonstrating that the model does not provide a complete understanding of all the diffusion or molecular motions in high molecular mass polymer melts, at least in its present form. The nanoparticles considered in this work are ideal for discerning the presence of other mobility mechanism besides reptation as the high degree of intramolecular crosslinking minimizes chain entanglements (the network chains/loops are too short), even for the high molecular mass nanoparticles.

The nanoparticles[2] considered here were found to produce anomalous flow behavior when blended with linear polymer.[28] Yet, this behavior depended strongly on the degree of crosslinking with light crosslinking producing no unusual effect while tight crosslinking yielded unusual rheological behavior. The purpose of the present work is thus two fold; to characterize these unique nanoparticles in dilute solution to determine their molecular architecture and to study the dynamics of polymer relaxation in this novel and ideal system as a function of that architecture.

Table 1. Number–Average Molecular Masses (M_n) and Polydispersity Index (PDI) of the Linear Precursors for the Lightly (2.5 mol % Crosslinker) and Tightly (20 mol % Crosslinker) Crosslinked Nanoparticles Together with Their Abbreviations

M_n (kDa)	% Crosslinker (mol %)	PDI	Abbreviation if Linear (Crosslinked)
24.5	2.5	1.14	24.5 kDa-2.5%-L (-X)
60.1	2.5	1.16	60.1 kDa-2.5%-L (-X)
158.0	2.5	1.40	158 kDa-2.5%-L (-X)
25.3	20.0	1.08	25.3 kDa-20%-L (-X)
52.0	20.0	1.18	52.0 kDa-20%-L (-X)
135.0	20.0	1.20	135 kDa-20%-L (-X)

EXPERIMENTAL

Materials

The synthesis of the nanoparticles and their linear analogs has been discussed previously.[2] Table 1 shows the molecular masses and polydispersity indices (PDI = weight to number–average molecular mass ratio) of the linear precursors for the *lightly* (2.5 mol % crosslinker) and *tightly* (20 mol % crosslinker) crosslinked nanoparticles used in this study, together with abbreviations. The molecular weights were determined using gel permeation chromatography relative to linear polystyrene standards. All polymers were dissolved in tetrahydrofuran (THF) and passed through a Waters chromatograph equipped with four 5-μm Waters columns (300 mm $\times$ 7.7 mm) connected in series with increasing pore size (100, 1000, 100,000, 1,000,000 Å).

Figure 1 illustrates the crosslinking process. The linear precursors are first dissolved in an excess of benzyl ether (BCB concentration $\sim$0.2 M) and then this solution is added drop wise to a reservoir of hot benzyl ether. The high temperature (T = 250 °C) initiates the crosslinking process and the ultradilute conditions (final BCB concentration $\sim$0.05 M) ensure that intermolecular crosslinking is minimized. Thus, the crosslinked nanoparticles potentially have the same molecular mass as the linear precursors. All the solvents were purchased from Sigma–Aldrich and used as received.

Intrinsic Viscosity

The solutions for the measurement of intrinsic viscosity were prepared at least 1 day before the measurement by dissolving the polymer in pure solvent. Before usage, the solution was filtered with a 1-μm filter to remove any undissolved impurities. The intrinsic viscosity was calculated by measuring the density of the solution, the flow time in a Cannon-Manning Semi-Micro viscometer (size 75) of the pure solvent and the solution, and the concentration of the solution. The measurements were made at low shear rates (typical flow times were close to 200 s), with four different concentrations, at a constant temperature of 35 °C. The data obtained was then analyzed using the two leading terms in the Huggins[29] and Kraemer[30] relations

$$\eta_{sp}/c = [\eta] + k_h[\eta]^2 c + \ldots \quad (3a)$$

and

$$\ln(\eta_{rel})/c = [\eta] - k_k[\eta]^2 c + \ldots \quad (3b)$$

where η_{sp} is the specific viscosity ($[\eta_{solution} - \eta_{solvent}]/\eta_{solvent}$), η_{rel}, the relative viscosity ($\eta_{solution}/\eta_{solvent}$), $[\eta]$, the intrinsic viscosity, c, the polymer concentration (g of polymer/mL of solution), and k_h and k_k, the Huggins and Kraemer coefficients (the values for these constants in THF and cyclohexane are given in Table A1), respectively. The $[\eta]$ values obtained from both these relations agreed within $\pm$2%; therefore, only the $[\eta]$ values obtained from the Huggins relation are reported in this paper.

For each of the different polymer nanoparticles and their linear analogs, the intrinsic viscosity was measured in five different solvents. Each solvent had a different solubility parameter (δ in $(cal/cm^3)^{1/2}$ at 25 °C) shown in parentheses: cyclohexane (8.2), toluene (8.9), THF (9.1), benzene (9.2) and chloroform (9.3).[31]

Light Scattering

The hydrodynamic radius (R_h) was measured using a Protein-Solutions Dynapro DLS instru-

ment. In the instrument, fluctuations in the intensity of the scattered light are related to the diffusion coefficient of the molecules (D_θ). Then, R_h is calculated from the diffusion coefficient using the Stokes–Einstein relation[32]

$$D_\theta = \frac{k_B T}{6\pi\eta_{solvent} R_h} \quad (4)$$

where k_B is the Boltzmann constant and T is the temperature. Thus, the R_h obtained from DLS data is the size of a spherical particle that would have a diffusion coefficient equivalent to that of the molecule tested.[33]

Again, all the solutions used for DLS were prepared at least 1 day before the measurement and filtered with a 0.1-μm filter to remove any undissolved impurities. To compare with the intrinsic viscosity measurements, all experiments were performed at 35 °C. Further, as R_h is a function of concentration[34–36] the extrapolated value to zero concentration (R_{h0}) was used and determined as described in the Appendix.

Neutron Scattering

The small angle neutron scattering (SANS) measurements were carried out using the 30-m NG3 and NG7 SANS instruments at the National Institute of Standards and Technology (NIST), Centre for Neutron Research (NCNR) in Gaithersburg, MD. Two instrument configurations were used. The first had five guides, a sample to detector distance of 600 cm with a 25 cm detector offset, giving a scattering vector (q) range of 0.0084–0.1136 Å^{-1}. The second configuration also had five guides, a sample to detector distance of 135 cm with a 25 cm detector offset, giving a q range of 0.018–0.47 Å^{-1}. Both configurations had a neutron wavelength of 6 Å with a 15% spread. All the measurements were performed at 35 °C, in deuterated solvents. The use of deuterated solvents greatly reduces the scattering time required for each solution by significantly enhancing the scattering contrast, even though this might slightly affect the polymer–solvent interactions. Several concentrations were used to examine the effect of concentration on R_g to determine the extrapolated value (R_{g0}). The modified Zimm analysis we used to account for this effect is provided in the Appendix.

Kratky and Guinier Plots

Further quantification of the molecular characteristics can be gleaned through careful consideration of neutron scattering data. The Debye function[37] is used to characterize polymer chains in the theta condition (second virial coefficient, $A_2 = 0$) and can describe scattering from polymer molecules in a good solvent. The scattering intensity (or differential cross section) $I(q)$ is given as[12,38]

$$I(q) = \phi \times V(\Delta\rho)^2\{2(\exp(-(qR_g)^2) + (qR_g)^2 - 1)/(qR_g)^4\} \quad (5)$$

Here, ϕ is the volume fraction of scattering centers, V, the volume of a single scattering center, $(\Delta\rho)^2$ the difference in the scattering length densities between solvent and scatterer (or the contrast) and q, the scattering vector ($4\pi/\lambda \times \sin(\theta/2)$; θ is the scattering angle and λ the neutron wavelength.). The term in the curly brackets is the form factor ($P(q)$) that describes how $I(q)$ is modulated by neutron interference effects from the different parts of the same scattering center. In the high q limit, eq 5 reduces to

$$I(q) \times q^2 = 2\phi \times V(\Delta\rho)^2/(R_g^2) \quad (6)$$

For a given sample, ϕ, V, $\Delta\rho$, R_g are constant; thus, from eqs 5 and 6, a plot of $I(q) \times q^2$ *vs.* q should asymptotically approach a plateau value at high q values for a Gaussian coil and is known as a Kratky plot. Deviations from the asymptotic behavior in the Kratky plot can be used as an indicator of the segment distribution within the system. Both ring and star polymers have a peak (maximum) prior to the asymptote revealing different distributions than linear polymers.[39] Indeed a gel-like crosslinked polymer nanoparticle has a large peak.[40] However, the high q limit is still a constant asymptote, as Gaussian chains are present between the robust crosslinks. Finally, a constant density sphere has no plateau and a series of ever decreasing peaks is seen. Thus, the Kratky plot shape is a good indicator of the molecular architecture and is used by us to infer particle-like nature.

In the low q scattering range, one can use the Guinier approximation, when $q \times R_g$ is small ($\ll 1$), and the scattering function can be written as

$$\log I(q) = \log I(0) - \frac{(qR_g)^2}{3} \quad (7)$$

where $I(0)$ is given by $\phi V(\Delta\rho)^2$. The Guinier plot,[41] $\log(I(q))$ *vs.* q^2, allows determination of

R_g, and further, can be used as a concentration check through the neutron intensity at zero wavevector.

Burchard's ρ-Ratio

An extremely useful, quantitative indicator of the molecular conformation and the segment density within a polymer molecule is Burchard's ρ-ratio,[42] which requires SANS (or other scattering) as well as hydrodynamic data. This ratio can be computed from the molecular architecture of the molecule without the knowledge of chemical details and is given by

$$\rho = R_{g0} / R_{h0} \tag{8}$$

The radius of gyration of a molecule is intimately related to the segment density variation $\rho(r)$ within the molecule (where r is the radial distance from the center of mass). For a spherical architecture one finds,

$$R_g^2 = \left(\int_0^R r^4 \rho(r) dr \right) \Big/ \left(\int_0^R r^2 \rho(r) dr \right) \tag{9}$$

where R is the radius of the sphere. Since a hard sphere is nondraining, one has $R = R_{h0}$ and finds $\rho = \sqrt{3/5} \approx 0.775$ while Gaussian coils have $\rho = 1.2$–1.6 depending on solvent conditions.[43]

Differential Scanning Calorimetry Measurements

A TA instruments Q-1000 differential scanning calorimeter (DSC) was used to perform all glass transition (T_g) measurements. All of the samples were subjected to at least three heating–cooling cycles, where each cycle consisted of heating the sample from 0 to 200 °C, at a rate of 5 °C/min, followed by cooling back to 0 °C, also at 5 °C/min. The inflection point for the heat flow as a function of temperature was taken as the glass-transition temperature for a particular cycle. The glass-transition temperatures reported in this work are the mean of the glass-transition temperatures obtained from the second and the third run cycles.

Rheology Measurements

The nanoparticles were molded by compression, under vacuum, in a pellet press (8 mm diameter) to ensure that no trapped air remained in the sample. The samples were then aged at 130–170 °C, under vacuum, for several hours. The 8-mm diameter discs obtained from the pellet press were placed on the 8-mm parallel plates fixture of a Rheometrics ARES rheometer set at a gap of ~0.4 mm. Measurements were done in the dynamic (oscillatory) mode. Frequency sweeps in the range 0.1–100 rad/s were performed at various temperatures (130–230 °C). These were then combined using time–temperature superposition[44] to yield a master curve at 170 °C (all quoted temperatures refer to the surface temperature of the lower plate).

RESULTS AND DISCUSSION

Hydrodynamic Properties

The utility of dilute solution viscosity measurements is well known.[45] More recently, Burchard[42] illustrates the importance of studying dilute solutions with a variety of techniques to fully understand a given system. Further, the polymer volume change with solvent under dilute conditions is a good indicator of the polymer–solvent thermodynamic interaction[46] which may be dependent on molecular architecture. The solvent in which the polymer has the greatest intrinsic viscosity (highest volume) is assumed to have the same solubility parameter as the polymer.[47] This method allows determination of the best solvent for the polymer as well as the change in the molecular volume with solvent type.

Figure 2 shows the intrinsic viscosity variation as a function of the solvent solubility parameter for the 52.0-kDa tightly crosslinked nanoparticle and linear analog as well as the 60.1-kDa lightly crosslinked nanoparticle. The intrinsic viscosity is made into a dimensionless ratio by the maximum intrinsic viscosity to compare the relative change in volume for each polymer.

It can be seen that the relative intrinsic viscosity for the tightly crosslinked nanoparticles varies between 0.64 (cyclohexane) and 1 (THF) while for the lightly crosslinked nanoparticles, it varies between 0.44 (cyclohexane) and 1 (benzene). On the other hand, for the linear precursors of the tightly crosslinked nanoparticles, it varies between 0.38 (cyclohexane) and 1 (benzene) revealing that the tightly crosslinked

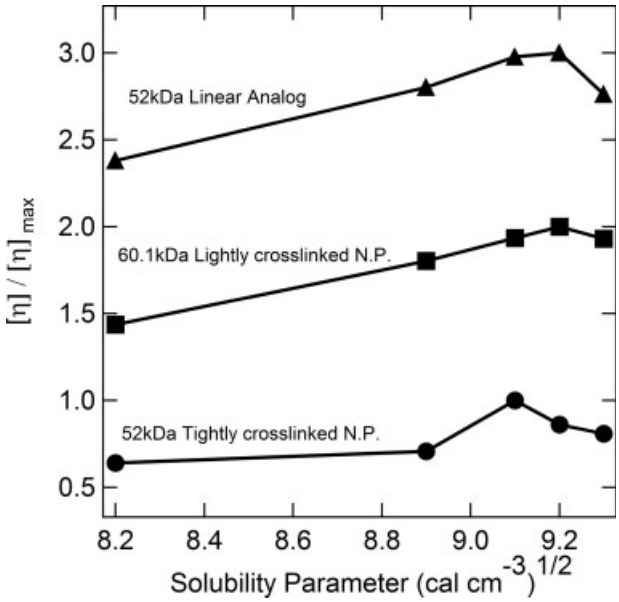

Figure 2. Intrinsic viscosity normalized with the maximum value plotted against solubility parameter at 35 °C. The data for the linear precursor (52.0 kDa-20%-L, triangles) and the lightly crosslinked nanoparticles (60.1 kDa-2.5%-X, squares) have been shifted by 2 and 1, respectively, from the tightly crosslinked nanoparticles' (52.0 kDa-20%-X, circles) data.

nanoparticles do not expand or contract as much as the lightly crosslinked particles or its linear analog.

Also, the linear analog and the lightly crosslinked 60.1-kDa nanoparticle have a maximum at a solubility parameter of 9.2 $(cal/cc)^{1/2}$ (benzene), while the tightly crosslinked particle has a maximum at 9.1 $(cal/cc)^{1/2}$ (THF). Thus, the degree of crosslinking has a slight effect on the polymer solubility parameter and hence the thermodynamic interactions between the nanoparticles and the solvents. However, these results clearly indicate that the solubility parameter for all the systems is quite close to that frequently quoted for linear polystyrene (9.1–9.2 $(cal/cm^3)^{1/2}$).[31]

When the viscosimetric radius was determined from the intrinsic viscosity (R_η)[46] and compared to the hydrodynamic radius, we found little difference. In Figure 3, the variation of the hydrodynamic radius with molecular mass in THF is shown for the lightly crosslinked nanoparticles, tightly crosslinked nanoparticles, and their linear analogs. The viscosimetric radius for polystyrene standards (Scientific Polymer Products) in THF is also shown. It can be seen that the linear analog has radius values within experimental error to pure polystyrene, indicating that the linear analog does indeed behave similarly to linear polystyrene. It can also be seen that the nanoparticles radius decreases with increasing crosslink density, with the linear analog being the largest and the tightly crosslinked nanoparticles the smallest in size. This suggests that, as may be expected, intramolecular crosslinking causes a collapse of the linear polymer chain. Also shown is the scaling for a constant density sphere, of equal density to bulk polystyrene, showing that the tightly crosslinked nanoparticles are not exactly equivalent to hard spheres when in solution.

Neutron Scattering

SANS was used to measure the radius of gyration of the particles in solution (due to a paucity of scattering time, measurements were carried out in *d*-THF (deuterated THF) and *d*-cyclohexane only). The raw SANS data was reduced to

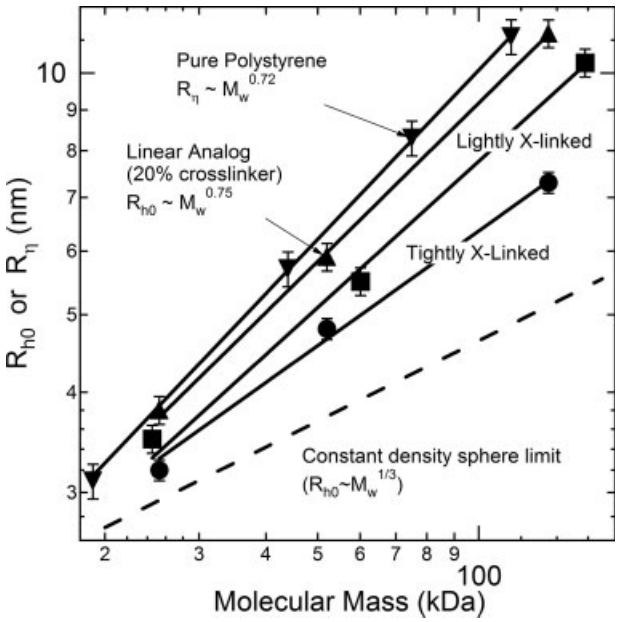

Figure 3. Scaling of the viscosimetric radius (R_η) and the extrapolated hydrodynamic radius (R_{h0}) with molecular mass. The data for the linear precursor (downward triangles) agrees well with that for polystyrene standards (upward triangles) while the lightly crosslinked (2.5% crosslinker, squares) and tightly crosslinked (20% crosslinker, circles) nanoparticles deviate significantly from the linear polymer scaling. However, neither approaches the scaling predicted for a hard sphere of density equal to that for bulk polystyrene.

Table 2. Radius of Gyration Determined from a Guinier Regression, Debye Flexible Polymer Fit, and Hard Sphere Fit As Well As the Hydrodynamic Radius for the Various Nanoparticles and Their Linear Precursors in *d*-THF (SANS Data) and THF (DLS Data)[a]

M_n (kDa)	% Crosslinker	Nature	Guiner Regression (nm)	Flexible Polymer Fit (nm)[b]	Hard-Sphere Fit (nm)[c]	R_h (nm)[d]	h[e]
25.3	20	Linear	2.5 ± 0.03	2.6 ± 0.04	NA	3.5 (3.7)	1
52	20	Linear	3.0 ± 0.02	2.8 ± 0.03	NA	5.4 (5.8)	1
135	20	Linear	3.0 ± 0.02	3.1 ± 0.03	NA	8.7 (11.2)	1
25.3	20	Crosslinked	2.0 ± 0.01	2.9 ± 0.06	1.9 ± 0.02	3.1 (3.2)	0.86
52	20	Crosslinked	2.3 ± 0.01	3.8 ± 0.05	2.4 ± 0.01	4.7 (4.8)	0.82
135	20	Crosslinked	3.4 ± 0.01	8.5 ± 0.05	3.9 ± 0.03	6.9 (7.3)	0.65
24.5	2.5	Linear	2.4 ± 0.02	2.6 ± 0.03	NA	3.5 (3.6)	1
60.1	2.5	Linear	2.8 ± 0.03	2.8 ± 0.04	NA	5.4 (5.7)	1
158	2.5	Linear	3.2 ± 0.02	3.1 ± 0.04	NA	9.2 (10.8)	1
24.5	2.5	Crosslinked	2.4 ± 0.01	2.5 ± 0.03	NA	3.3 (3.5)	0.97
60.1	2.5	Crosslinked	2.8 ± 0.01	3.0 ± 0.02	NA	5.0 (5.5)	0.96
158	2.5	Crosslinked	3.5 ± 0.02	3.4 ± 0.03	NA	8.7 (10.3)	0.95

[a] Concentration is 5 mg/mL and temperature is 35 °C. Corresponding values with *d*-cyclohexane and cyclohexane as the solvents are provided in the Appendix (Table A2).
[b] Debye flexible polymer fit: $I(q) = \varphi V(\Delta\rho)^2 \{2 \exp(-(qR_g)^2 + (qR_g)^2 - 1)/(qR_g)^4\}$.
[c] Hard-sphere fit: $I(q) = \varphi V(\Delta\rho)^2 \{3(\sin(qR) - qR\cos(qR))/(qR)^3\}^2$; $R_g = \sqrt{3/5} \times R$, R is the sphere radius.
[d] R_{h0} values are shown in parentheses.
[e] $h = R_{h0}$ (crosslinked nanoparticle)/R_{h0} (linear polymer).

an absolute scale (I (cm^{-1}) *vs.* q ($Å^{-1}$)) using the standard NIST procedure (typical I (cm^{-1}) *vs.* q ($Å^{-1}$) graphs obtained after normalization have been shown in the Fig. A1). To determine the molecular size (radius of gyration), each absolute data set was then analyzed by fitting to both the Debye equation (Gaussian coil fit) as well as the hard sphere form factor. The fits obtained from both these equations were compared with the R_g values obtained from the Guinier plots. The fitting results for the Gaussian coil model (typical fits of the data with the Debye model have been shown in the Fig. A1), hard sphere model as well as the Guinier radii for the samples in *d*-THF, are given in Table 2.

It can be seen that the Guinier fits for the lightly crosslinked nanoparticles and the linear analogs compare well with the fits obtained from the Debye equation for flexible polymers, showing that the lightly crosslinked particles as well as the linear precursors indeed behave similar to a Gaussian coil in solution. However, the data for the tightly crosslinked particles could not be accurately fitted with the Debye equation. Instead, their Guinier radii were found to be close to the radii obtained by fitting the data to a hard sphere model.

Defining the contraction as the ratio of hydrodynamic radii of the NPs, with respect to the linear precursor, at zero concentration (h, Table 2), one can see that the size of the nanoparticles is greatly reduced on crosslinking. For Antonietti et al.'s microgels,[8] which had 1 in every 10 monomer units (on average) crosslinked, the h value varied between 0.96 and 0.98. In comparison, the lightly X-linked NPs have h values similar to those reported in their work, whereas the tightly X-linked NP has an h value between 0.65 and 0.86. Thus, the use of a larger amount of BCB as the crosslinking agent[2] does provide greater reduction in nanoparticle volume as compared to *p*-bis(chloromethyl) benzene.[8]

Burchard's ρ-ratio (R_{g0}/R_{h0}) is shown in Figure 4 as a function of the molecular mass for both the tightly and lightly crosslinked nanoparticles. The Gaussian coil and the hard sphere (constant density) limits are also shown. It is seen that the lightly crosslinked nanoparticles always have a value close to or within the range determined for a Gaussian coil. The tightly crosslinked nanoparticles, however, always have a value between the hard sphere and the Gaussian coil limits. Also, the ratio decreases with increasing molecular mass showing a shift toward the hard sphere limit. Thus, particle-like behavior for the tightly crosslinked nanoparticles is suggested, which becomes more apparent as the molecular mass is increased.

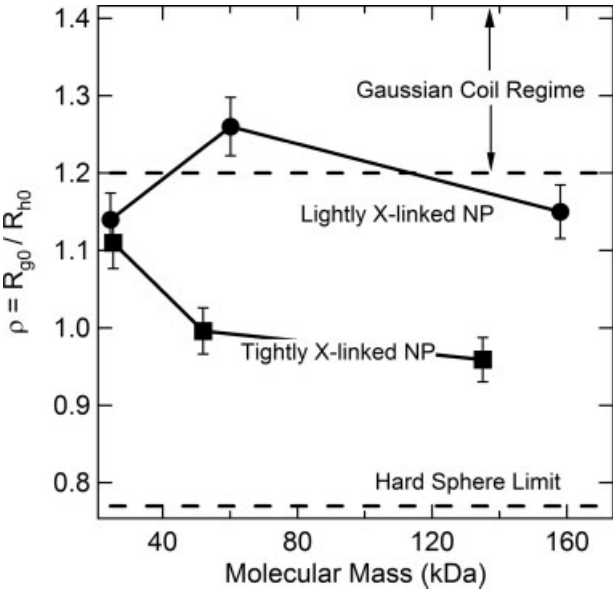

Figure 4. Burchard's ρ-ratio (ratio of radius of gyration to hydrodynamic radius) variation for the lightly (2.5% crosslinked, circles) and tightly crosslinked (20% crosslinked, squares) nanoparticles with molecular mass in THF at 35 °C. A nondraining hard sphere should have a value of 0.775 while a Gaussian coil has a range of values depending upon solvent conditions. The lightly crosslinked nanoparticles behave similar to coil while the tightly crosslinked nanoparticles approach the hard sphere limit, particularly at higher molecular mass.

The neutron scattering data were also used to construct Kratky plots for both the lightly and tightly crosslinked nanoparticles. The Kratky plot for the lightly crosslinked nanoparticles [Fig. 5(a)] demonstrates the behavior expected for a Gaussian coil. The data for the tightly crosslinked nanoparticles [Fig. 5(b)], on the other hand, shows a peak in the Kratky plots, indicative of particle-like behavior. It is also seen that the peak becomes more pronounced with increasing molecular mass of the tightly crosslinked nanoparticles. This trend further supports the shift toward particle-like behavior with increasing molecular mass as seen with the ρ-ratio values (Fig. 4).

Note though that there is a plateau at large wavevector, q, seen in Figure 5(b). Hence, the overall segment distribution is apparently Gaussian; however, it is organized in such a manner as to give a maximum due to constraints contributed by the crosslinked monomer units. Modeling of the segment distribution more than this is beyond the scope of this work. Clearly, assumptions would have to be made regarding the segment distribution and possibly larger wavevector data would be needed to determine the pair distribution function and to perform detailed analysis. However, the peak in the Kratky plot together with the suppressed ρ-ratio and smaller variation of intrinsic viscosity with solvent change clearly indicate particle-like behavior.

Certainly the degree of crosslinking has an effect on the ultimate molecular morphology developed, as expounded above. However, the results in Figures 4 and 5(b) suggest that molecular mass affects the segment density distribution and hence morphology. By recalling the work of Kuhn and Balmer[3] and Kuhn and Majer,[48] we note that the average number of statistical segments in a cycle, $\langle k \rangle$, at small degree of intramolecular crosslinking, is related to the number of statistical segments in a molecule, N, by

$$\langle k \rangle = 2\sqrt{2/3} \times \sqrt{N} \approx \sqrt{N}$$

One may expect that the initial cycles formed in the intramolecularly crosslinked nanoparticles will have 35 monomer units for the 25.3-kDa

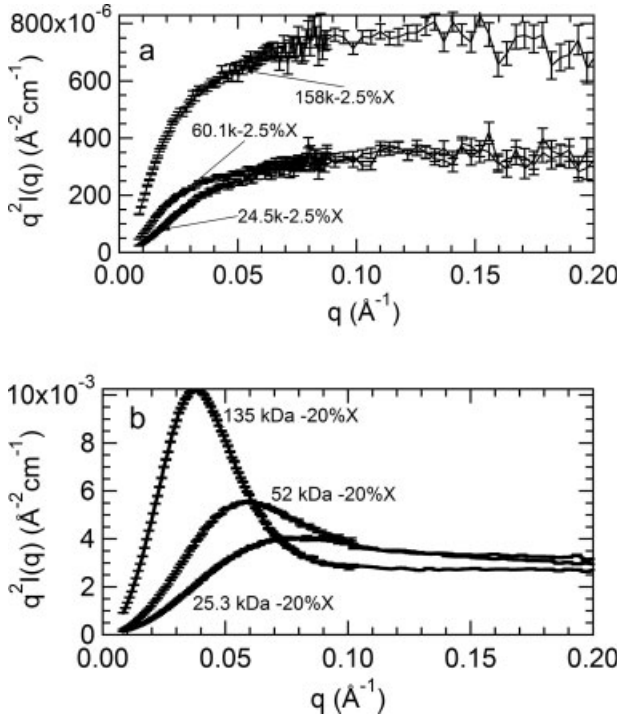

Figure 5. Kratky plots for the lightly crosslinked (a) and the tightly crosslinked nanoparticles (b). The data was obtained in d-THF at 35 °C, and a concentration of 5 mg/mL. A peak in the Kratky plot is indicative of particle-like behavior, while a plateau is expected for a Gaussian coil.

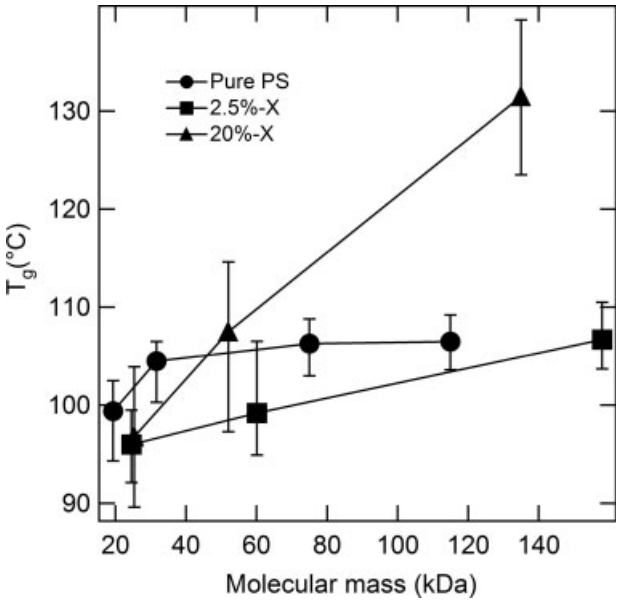

Figure 6. The glass-transition temperatures for both the lightly and tightly crosslinked nanoparticles compared to pure linear polystyrene. The error bars represent the spread of the transition, indicating its beginning and end.

tightly crosslinked nanoparticle and increase to ~80 for the highest molecular mass, 135 kDa (there are five monomer units in a statistical segment[31]). This phenomenon could affect the ultimate molecular morphology after crosslinking is completed and could account for the decrease in the ρ-ratio with molecular mass shown in Figure 4. We also note the ring polydispersity,[48] $<k^2>^{1/2}/<k>$, is ~0.46 $N^{1/4}$ and so higher mass molecules could potentially have a greater difference in initial ring size. These effects are noted here as they could affect the ultimate molecular morphology and final molecular properties surely deserving more attention in future studies since our system is simpler to study in terms of molecular "folding" than polypeptides.[49]

Bulk Properties

The thermal analysis performed on both the lightly and tightly crosslinked nanoparticle systems also reinforces the observations above. It can be seen from Figure 6 that the glass transition for both the lightly and tightly crosslinked particles increases with increasing molecular mass (the error bars represent the beginning and the end of the glass transition). Also, the T_g for the tightly crosslinked nanoparticles is always greater than the T_g of the lightly crosslinked nanoparticles of similar molecular mass. It should be noted that the increase in T_g, caused by the intramolecular crosslinking of polystyrene, although significant, is still less than the elevation caused in polystyrene networks formed by the copolymerization of polystyrene and divinylbenzene[50,51], as has been seen before.[8] For example, Nielsen[52] developed a simple relation to find the glass-transition temperature rise due to crosslinking: 39 kDa-°C/M_x, where M_x is the molecular mass between crosslinks. One would expect a 9 °C (lightly crosslinked) and 75 °C (tightly crosslinked) increase above T_g for the equivalent linear polymer, which is clearly not the case. In fact, a slight T_g *decrease* may be apparent for the lightly and tightly crosslinked nanoparticles at low molecular weight. Thus, the discrete crosslinked nature of the bulk nanoparticles clearly affects the glass-transition temperature in unusual ways.

Furthermore, it was seen before that addition of the tightly crosslinked nanoparticles caused a decrease in the glass-transition temperature of linear polystyrene.[28] This observation is quite interesting and contrary to the general mixing rule considering that high molecular mass linear PS has a T_g of ~106 °C, while the 135 kDa-20%-X NPs have a T_g of ~132 °C and a 1% blend of the nanoparticles in linear polymer was found to have a T_g of 103.5 °C.[53]

The complex viscosity as a function of frequency is shown for a three-arm polystyrene star (molecular mass for each branch ~108 kDa) and linear polystyrene (molecular mass 19.3 kDa, 75 kDa, 115 kDa), [Fig. 7(a)], and the lightly [Fig. 7(b)] and tightly [Fig. 7(c)] crosslinked nanoparticles (the data has been shifted to 170 °C using time–temperature superposition[14]; the shift factors have been tabulated in the Table A3). Clearly, the rheological behavior of the crosslinked nanoparticles does not match the behavior observed for the linear or star-shaped polystyrene. Also, from Figure 7(c) it is apparent that only the lowest molecular mass (25.3 kDa) tightly crosslinked nanoparticle shows a terminal viscosity. All of the higher molecular mass tightly crosslinked nanoparticles in fact show a gel-like behavior, which is to be expected for a crosslinked network.[10] Note that we tried to measure the melt surface tension[55,56] of the 25.3 kDa-20%-X-NP sample. At 220 °C we found that the surface tension was extremely large and of order 150 mN/m, while linear polystyrene should have a surface tension of order 20 mN/m at this

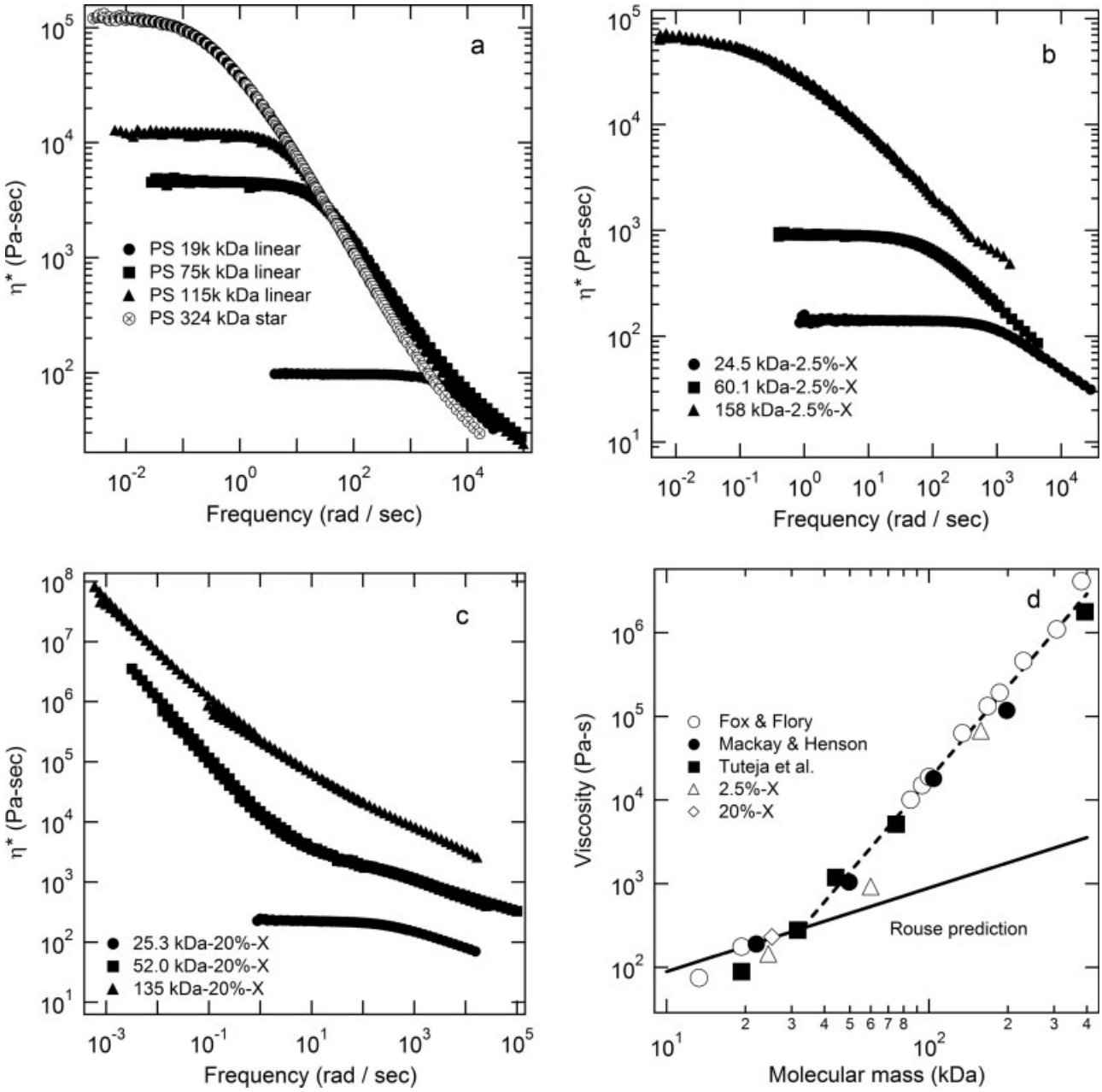

Figure 7. The complex viscosity as a function of frequency at 170 °C, for the three-arm polystyrene star and linear polystyrene (a), lightly crosslinked (b), and tightly crosslinked (c) nanoparticles. Increasing molecular mass and crosslink density causes an increase in the zero shear viscosity. A gel-like behavior is evident for the high molecular mass, tightly crosslinked nanoparticles. (d) The zero shear viscosity as a function of molecular mass (M) for polystyrene melts at 170 °C. Data from Fox and Flory,[15,16] Mackay and Henson,[54] and Tuteja et al.[53] are used. The zero shear viscosities for the pure lightly and tightly crosslinked nanoparticles are also shown (a zero shear viscosity is not observed for the 52 kDa-20%-X and 135 kDa-20%-X NPs).

temperature. We conclude that this sample must have a terminal modulus or yield stress that is small and probably less than 10 Pa. So this sample may be similar to the higher mass 20%-X-NP samples, with a gel-like behavior, that is disrupted in the rheological testing.

The observation of gel-like behavior for relatively low molecular mass tightly crosslinked

nanoparticles is in contrast to the behavior seen by Antonietti et al.[12] In their work, a zero shear viscosity was observed even for very high molecular mass ($M_w = 1.03 \times 10^6$, $R = 7.3$ nm) microgels.[12] However, the microgels only had 1 in every 10 monomer units crosslinked and the higher degree of crosslinking present in this work can cause a significant impediment to the motion of the small chains between the crosslinks. Antonietti et al. postulated that the viscosity behavior was linked to the cooperative nature of the crosslinked loops' motion. Thus, the gel-like behavior we observe may be expected, and it is certainly affected by the intramolecular crosslink density and nanoparticle size (or molecular mass).

The zero shear viscosity as a function of molecular mass for linear polystyrene at 170 °C is shown in Figure 7(d) together with the values for the lightly and tightly crosslinked nanoparticles. The lightly crosslinked nanoparticles may have a lower zero shear viscosity as compared to linear polystyrene of similar molecular weight,[12] suggesting easier mobility of the crosslinked molecule as compared to the linear chains; however, this is a tentative conclusion.

The modes for polymer relaxation and the effects of the relative motion of crosslinked loops become clearer by viewing the storage modulus data. The storage and loss modulus as a function of frequency for the three-arm polystyrene star and linear polystyrene of comparable molecular mass to the lightly and tightly crosslinked nanoparticles is shown in Figure 8, together with the nanoparticles' data. All of the lightly crosslinked nanoparticles as well as the 25 kDa-20%-X-NP show typical terminal zone behavior with $G' \sim \omega^2$ and $G'' \sim \omega^1$ at low frequencies (ω), with the caveat that the 20% crosslinked system may have a delicate gel-like behavior.

On increasing the molecular mass for the lightly crosslinked nanoparticles, the development of a plateau zone (corresponding traditionally to the presence of entanglements) can be seen and an ~10% increase in the plateau modulus is observed (determined through the minima in tan $\delta = G''/G'$[57]). Traditionally, the plateau modulus corresponds to the entanglement density present in polymer melts. Clearly, reptation motion, at least the way it is thought of traditionally, cannot account for the rheological behavior observed in these crosslinked particles, even though the rheological spectra of higher molecular mass lightly crosslinked nanoparticles is similar to the spectra obtained for higher molecular mass entangled linear polymers.

This trend is reinforced as we look at the rheological behavior of the tightly crosslinked nanoparticles. As the number of crosslinked loops present in the molecule increase from ~25/molecule (25.3 kDa-20%-X-NP) to ~50/molecule (52 kDa-20%-X-NP), a distinct change in the terminal behavior of the molecules is observed. With the increasing number of crosslinked loops, the storage modulus becomes essentially constant with respect to frequency (for low frequencies), a behavior typical of gels.[12] At this point it can be imagined that the large number of intramolecularly crosslinked loops present in the molecule cannot move cooperatively to allow for the molecules' relaxation; and essentially a high stress (yield stress) is required to allow for the loops to move together and hence for the molecule to relax. Further, the molecules become more particle-like with increasing molecular mass, as discussed above, probably contributing to the gel-like flow properties.

The observation of a constant storage modulus at low frequency as shown in Figure 8(c), also provides some interesting insights about the nature of the crosslinked particles. As can be seen, the modulus at low frequency increases with increasing nanoparticle molecular weight (radius), with the caveat that the lowest molecular weight sample, 25.3 kDa-20%-X, has a very small terminal modulus as determined through our surface tension measurements.[55] However, predictions of flocculated suspensions show that modulus should scale inversely to the particle radius raised to a power[58,59]; indeed, even jammed particle systems, at zero temperature, show a scaling inversely proportional to the radius raised to the power of the system dimensionality.[60] The modulus increase seen in our system may then be related to two factors. First, our results above point to the fact that the larger molecular weight system is more "particle-like" in nature which can be expected to influence the flow properties (as demonstrated by the other rheological properties). Secondly, the glass temperature for the 135 kDa-20%-X system is ~25 °C higher than that for the 52.0 kDa-20%-X. For a given testing temperature, 170 °C in our case, this would tend to increase the flow properties by a factor of ~30–40, accounting for the observed trend.

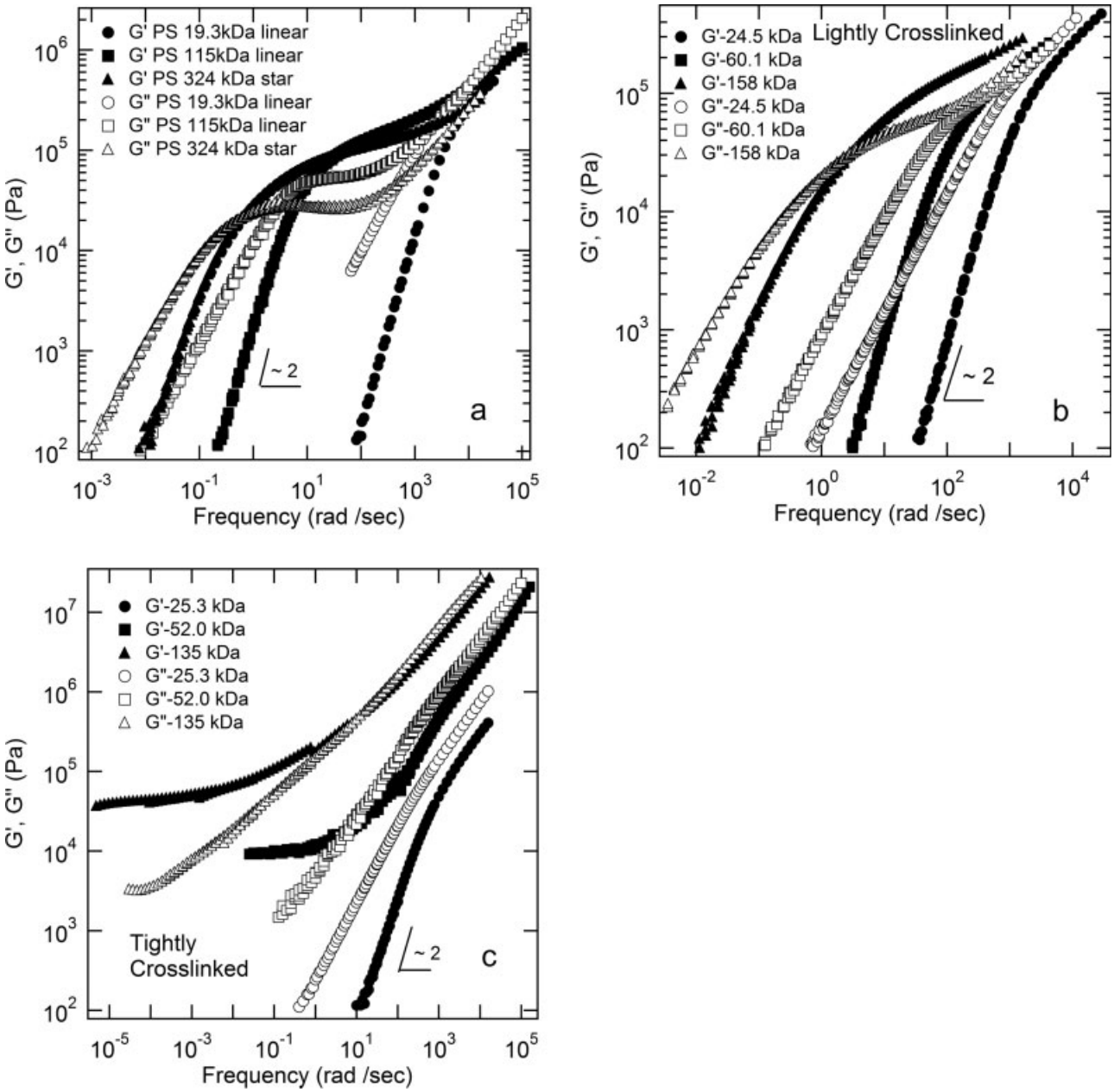

Figure 8. The storage (G') and loss (G'') modulus as a function of frequency for the three-arm polystyrene star and linear polystyrene (a), lightly crosslinked (b), and tightly crosslinked (c) nanoparticles, at 170 °C. A terminal zone behavior similar to linear polymers is evident for all of the lightly crosslinked nanoparticles, while a transition zone behavior similar to linear polymers is evident for both the lightly and tightly crosslinked nanoparticles.

CONCLUSIONS

An innovative synthesis process was used to induce intramolecular crosslinks within linear polystyrene. It was seen from intrinsic viscosity and DLS measurements that crosslinking causes a decrease in the size of the chain and also that the tightly crosslinked nanoparticles have much limited changes in dimensions between different solvents as compared to the lightly crosslinked and linear precursor chains. This demonstrates that intramolecular crosslinking limits the expansion and contraction of the molecule.

SANS was used to show that the lightly crosslinked nanoparticles and the linear precursors behave like Gaussian coils in solution. On the other hand, the tightly crosslinked nanoparticles showed a peak in the Kratky plot indicative of particle-like behavior. It was also seen that the peak in the Kratky plot becomes more pronounced with increasing molecular mass of the nanoparticles. This trend was reinforced by determining Burchard's ρ-ratio for the various nanoparticles. It was seen that the ρ-ratio values for lightly crosslinked particles are indeed close to the Gaussian range while the values for tightly crosslinked nanoparticles were seen to move toward the hard sphere limit with increasing molecular mass.

These molecules were ideal to study the rheological/relaxation behavior of high molecular mass polymers in the absence of entanglements; as the high crosslink density present in these molecules should influence entanglement coupling. It was seen that these molecules show most of the rheological characteristics of both unentangled and entangled polymeric systems. The terminal viscosity increased with increasing molecular mass and increasing crosslink density (contrary to earlier observations for particles with lower intramolecular crosslinking densities),[12] with the limiting case of high molecular mass samples with high degree of intramolecular crosslinking showing gel like behavior, with an infinite terminal viscosity. It was postulated that the mobility of these molecules is not governed by the motion of individual chains, but rather by the cooperative and relative motion of the crosslinked loops present in the system in accord with Antonietti et al.'s[12] hypothesis. This type of motion is indeed intuitive, as the crosslinking present between the molecules must cause many of the loops to move together.

It can then be said that the reptation model (or the presence of a tube for relaxation) does not explain many of the important rheological features seen for our systems. Clearly, coupling or cooperative motion has to play a significant nature in the relaxation processes of these molecules. Indeed, Schweizer[61,62] postulated a coupling theory for polymers which predicts many of the polymer relaxation modes observed experimentally.

Funding from NSF CTS-0442115, NSF NIRT-0210247, MRL at UCSB and DMR05-20415 are gratefully acknowledged. This work was also supported by the U.S. Department of Energy, BES-Materials Science, under contract No. W-31-109-ENG-38 to the University of Chicago for the neutron scattering experiments conducted at Argonne National Laboratory. The authors also thank Denis Wozniak and Dr. P. Thiyagarajan for their assistance with the SANS experiments.

APPENDIX

Huggins and Kraemer Coefficients

Equation 3 can be used to calculate the Huggins and Kraemer coefficients through intrinsic viscosity measurements. Table A1 shows the variation of Huggins and Kraemer coefficients with molecular weight for the 2.5 and 20% crosslinked nanoparticles in THF and cyclohexane, at 35 °C.

Modified Zimm and Yamakawa Approaches to Size Variation of Macromolecules

The Zimm equation is written[38,63]

$$K_1/I(q) = \{1 + 1/3 \times q^2 R_{g0}^2\}/cM + 2 \times A_2$$

where k_1 is $[\Delta\rho]^2/N_A\ {\rho_m}^2$, with ρ_m being the mass density of the scatterer. This equation can be arranged to

$$\log(I) = \ln(C_0) - \log(1 + 1/3 \times q_2 R_{g0}^2 /\{1 + 2 \times A_2 cM\})$$

$$\approx \ln(C_0) - 1/3 \times q_2 R_{g0}^2 /\{1 + 2 \times A_2 cM\}$$

where C_0 is a grouping of variables that is constant for a given system and concentration. Per-

Table A1. Variation of Huggins and Kraemer Coefficients with Molecular Weight for the 2.5% and 20% Crosslinked Nanoparticles in THF and Cyclohexane, at 35 °C

Molecular Weight (Da)	THF		Cyclohexane	
	k_h	k_k	k_h	k_k
Tightly crosslinked				
25,300	1.24	−0.55	2.57	−1.8
52,000	0.64	−0.13	2.97	−0.23
135,000	0.23	0.26	NA[a]	NA[a]
Lightly crosslinked				
24,500	0.62	0.003	NA	NA
60,100	0.58	0.0	0.82	−0.55
158,000	0.49	0.005	0.57	−0.33

[a] The 135-kDa tightly crosslinked nanoparticles had a very low solubility (<1 mg/mL) in cyclohexane.

Table A2. Radius of Gyration Determined from a Guinier Regression, Debye Flexible Polymer Fit, As Well As the Hydrodynamic Radius for the Various Nanoparticles and Their Linear Precursors in *d*-Cyclohexane (SANS Data) and Cyclohexane (DLS Data)[a]

Molecular Weight(kDa)	% Crosslinker	Nature	Guiner Radius (nm)	Flexible Polymer Fit (nm)[b]	R_h[c] (nm)
25.3	20.0	Linear	4.6 ± 0.02	5.0 ± 0.02	3.0 (4.2)
52.0	20.0	Linear	7.0 ± 0.05	7.8 ± 0.02	4.7 (6.7)
135.0	20.0	Linear	8.6 ± 0.11	8.8 ± 0.05	8.0 (9.1)
25.3	20.0	X-linked	NA[b]	NA[b]	NA[b] (2.8)
52.0	20.0	X-linked	NA[b]	NA[b]	NA[b] (3.7)
135.0	20.0	X-linked	NA[b]	NA[b]	NA[b] (5.9)
24.5	2.5	Linear	4.8 ± 0.02	5.0 ± 0.01	2.6 (4.2)
60.1	2.5	Linear	7.8 ± 0.01	8.5 ± 0.01	5.3 (7.1)
158.0	2.5	Linear	7.8 ± 0.04	8.7 ± 0.02	7.8 (8.3)
24.5	2.5	X-linked	5.3 ± 0.01	5.0 ± 0.02	2.5 (4.1)
60.1	2.5	X-linked	6.1 ± 0.03	6.6 ± 0.02	5.2 (6.4)
158.0	2.5	X-linked	7.7 ± 0.02	8.0 ± 0.03	8.0 (9.1)

[a] Concentration is 5 mg/mL and temperature is 35°C.
[b] The tightly crosslinked nanoparticles were insoluble in cyclohexane at this high concentration.
[c] Numbers in parentheses are the extrapolated values to zero concentration.

forming a Guinier analysis on the scattering data at low q will yield an apparent radius of gyration, R_g, which is given by

$$R_g^{-2} = R_{g0}^{-2} \times \{1 + 2 \times A_2 cM\} \qquad \text{(A1)}$$

Thus, a plot of the inverse square of the apparent radius of gyration *vs.* concentration will yield the true radius of gyration, R_{g0}, at zero concentration. This equation is useful when only a few concentrations are available for analysis thereby not warranting a full Zimm analysis and explains the (apparent) radius of gyration variation with concentration. This extrapolation procedure was used by us to determine R_{g0} and yielded good linear regression.

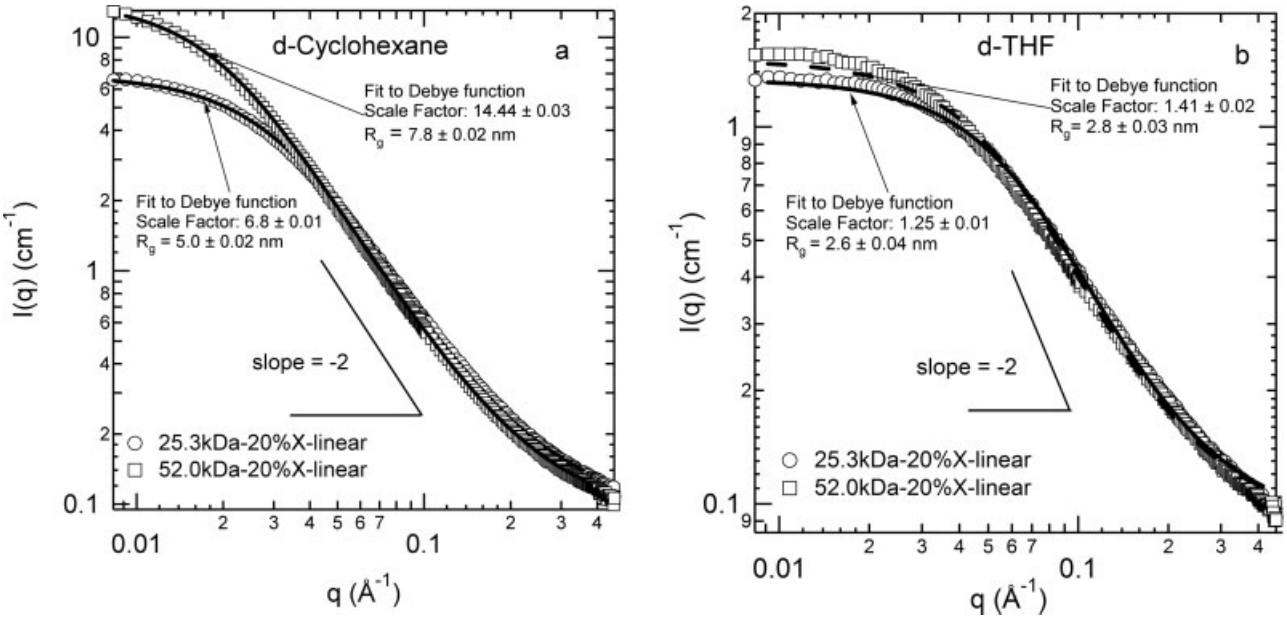

Figure A1. Typical I (cm^{-1}) *vs.* q (Å^{-1}) graphs obtained after normalization of the SANS data in *d*-cyclohexane and *d*-THF. The data was obtained at 35 °C, and the concentration was 5 mg/mL. The fits to the Debye function for the obtained data are also shown.

Table A3. Shift Factors[14] as a Function of Temperature for Linear Polystyrene, Lightly and Tightly Crosslinked Nanoparticles

	Temperature (°C)	a_T		Temperature (°C)	a_T
Linear polystyrene				160	2.89
Linear PS 19k				170	1.00
	130	284.00		180	0.41
	140	45.80		190	0.20
	150	10.30		200	0.10
	160	4.12		210	0.05
	170	1.00	158 kDa-2.5%-X	150	15.40
	180	0.26		160	3.45
Linear PS 75k	130	881.00		170	1.00
	140	85.20		180	0.35
	150	14.80		190	0.15
	160	3.44		200	0.08
	170	1.00		210	0.05
	180	0.35		220	0.03
	190	0.14	*Tightly crosslinked*		
	200	0.07	25.3 kDa-20%-X	130	155.00
Linear PS 115k	130	966.00		140	35.80
	140	92.00		150	6.93
	150	15.10		160	2.23
	160	3.48		170	1.00
	170	1.00	52 kDa-20%-X	130	982.00
	180	0.35		140	131.00
	190	0.14		150	39.15
	200	0.06		160	10.10
Lightly crosslinked				170	1.00
24.5 kDa-2.5%-X	130	310.00		180	0.21
	140	51.10		190	0.02
	150	11.10	135 kDa-20%-X	150	75.40
	160	3.04		160	12.50
	170	1.00		170	1.00
	180	0.24		180	0.35
	190	0.09		190	0.08
60.1 kDa-2.5%-X	140	44.70		200	0.05
	150	10.10		210	0.02

Yamakawa[34] applied nonequilibrium thermodynamics to determine the translational diffusivity, and hence R_h, as a function of concentration via

$$R_h^{-1} = R_{h0}^{-1} \times \{1 + k_D C\} \quad \text{(A2)}$$

where the subscript "0" is again the zero concentration value and k_D is a constant. This relation was used by us to determine the true hydrodynamic radius.

Radius of Gyration Variation in Cyclohexane

The radius of gyration determined from a Guinier regression, Debye flexible polymer fit, as well as the hydrodynamic radius for the various nanoparticles and their linear precursors in *d*-cyclohexane is provided in Table A2.

SANS Intensity Data After Normalization

The scattering intensity as a function of the wavevector q for the 25.3 kDa and 52.0 kDa-20%X-linear precursors in *d*-cyclohexane and *d*-THF at 35 °C, as reference to typical data obtained after normalization, yet without background subtraction, is shown in Figure A1. As can be seen in the figure, the data is fitted well by Debye function. All of the scattering data except for the data obtained for the tightly crosslinked nanoparticles could be fitted quite well with the Debye function.

Shift Factors for Rheological Data

The shift factors[14] (a_T) at various temperatures used for the time–temperature superposition of

data shown in Figures 7 and 8 are listed in Table A3. It can be seen that the shift factors for both the lightly and tightly crosslinked nanoparticles are similar to the shift factors for linear polystyrene. Note that the glass-transition temperature for the crosslinked nanoparticles is different from that of linear polymer (Fig. 6), accounting for some differences in the shift factors for a given temperature.

REFERENCES AND NOTES

1. Xia, Y. G. B.; Yin, Y.; Lu, Y. Adv Mater 2000, 12, 693–713.
2. Harth, E.; VanHorn, B.; Lee, V. Y.; Germack, D. S.; Gonzales, C. P.; Miller, R. D.; Hawker, C. J. J Am Chem Soc 2002, 124, 8653–8660.
3. Kuhn, W.; Balmer, G. J Polym Sci 1962, 57, 311–319.
4. Longi, P. G. F.; Rossi, U. Makromol Chem 1969, 129, 157.
5. Martin, J. E.; Eichinger, B. E. Macromolecules 1983, 16, 1345–1350.
6. Martin, J. E.; Eichinger, B. E. Macromolecules 1983, 16, 1350–1358.
7. Eichinger, B. E. Macomolecules 1980, 13, 1–11.
8. Antonietti, M.; Sillescu, H.; Schmidt, M.; Schuch, H. Macromolecules 1988, 21, 736–742.
9. Antonietti, M.; Ehlich, D.; Folsch, K. J.; Sillescu, H.; Schmidt, M.; Lindner, P. Macromolecules 1989, 22, 2802–2812.
10. Antonietti, M.; Bremser, W.; Schmidt, M. Macromolecules 1990, 23, 3796–3805.
11. Antonietti, M.; Bremser, W.; Pakula, T. Acta Polym 1995, 46, 37–44.
12. Antonietti, M.; Pakula, T.; Bremser, W. Macromolecules 1995, 28, 4227–4233.
13. Roland, C. M.; Santangelo, P. G.; Antonietti, M.; Neese, M. Macromolecules 1999, 32, 2283–2287.
14. Ferry, J. D. Viscoelastic Properties of Polymers, 3rd ed.;Wiley: New York, 1980.
15. Fox, T. G.; Flory, P. J. J Am Chem Soc 1948, 70, 2384–2395.
16. Fox, T. G.; Flory, P. J. J Polym Sci 1954, 14, 315–319.
17. Berry, G. C.; Fox, T. G. Adv Polym Sci 1968, 5, 261–357.
18. Edwards, S. F. Proc Phys Soc 1967, 92, 9.
19. deGennes, P. G. J Chem Phys 1971, 55, 572–579.
20. Lodge, T. P.; Rotstein, N. A.; Prager, S. Adv Chem Phys 1990, 79, 1–132.
21. McKenna, G. B.; Hadziioannou, G.; Lutz, P.; Hild, G.; Strazielle, C.; Straupe, C.; Rempp, P.; Kovacs, A. J. Macromolecules 1987, 20, 498–512.
22. Fetters, L. J.; Kiss, A. D.; Pearson, D. S.; Quack, G. F.; Vitus, F. J. Macromolecules 1993, 26, 647–654.
23. Antonietti, M.; Sillescu, H. Macromolecules 1986, 19, 798–803.
24. Koppi, K. A.; Tirrell, M.; Bates, F. S.; Almdal, K.; Mortensen, K. J Rheol 1994, 38, 999–1027.
25. Kornfield, J. A.; Fuller, G. G.; Pearson, D. S. Macromolecules 1989, 22, 1334–1345.
26. Doi, M.; Pearson, D.; Kornfield, J.; Fuller, G. Macromolecules 1989, 22, 1488–1490.
27. Ylitalo, C. M.; Kornfield, J. A.; Fuller, G. G.; Pearson, D. S. Macromolecules 1991, 24, 749–758.
28. Mackay, M. E.; Dao, T. T.; Tuteja, A.; Ho, D. L.; Horn, B. V.; Kim, H.-C.; Hawker, C. J. Nat Mater 2003, 2, 762–766.
29. Huggins, M. L. J Am Chem Soc 1942, 64, 2716.
30. Kraemer, E. O. Ind Eng Chem 1938, 30, 1200.
31. Brandrup, J.; Immergut, E. H. Polymer Handbook, 3rd ed.;Wiley: New York, 1989.
32. Einstein, A. Ann Phys (Leipzig) 1906, 19, 371–381.
33. In pp The hydrodynamic radius (R_h) and viscosimetric radius (R_η), determined from the viscosimetric volume, are almost equivalent. R_h is measured in a homogeneous flow field and R_η within a shear flow field. As long as the molecular distortion is not too great they appear to be practically the same.
34. Yamakawa, H. Modern Theory of Polymer Solutions;Harper & Row: London, 1971.
35. Munch, J. P.; Hild, G.; Candau, S. Macromolecules 1983, 16, 71–75.
36. Brown, W. Macromolecules 1985, 18, 1713–1719.
37. Debye, P. J Phys Coll Chem 1947, 51, 18–32.
38. King, S. M. In Modern Techniques for Polymer Characterisation; Pethrick, R. A.; Dawkins, J. V., Eds.; Wiley: New York, 1999.
39. Higgins, J. S.; Benoît, H. C. Polymers and Neutron Scattering.Clarendon Press: Oxford, 2002.
40. Kajiwara, K.; Burchard, W. Polymer 1981, 22, 1621–1628.
41. Guinier, A. F. G. Small Angle Scattering of X-rays;Wiley: New York, 1955.
42. Burchard, W. Adv Polym Sci 1999, 143, 113–195.
43. Schmidt, M.; Burchard, W. Macromolecules 1981, 14, 210–211.
44. Horio, M.; Fujii, T.; Onogi, S. J Phys Chem 1964, 68, 778.
45. Staudinger, H.; Heuer, W. Ber 1930, 63, 222–234.
46. Flory, P. J. Principles of Polymer Chemistry;Cornell University Press: Ithaca, 1953.
47. Jeong, M.; Mackay, M. E.; Hawker, C. J.; Vestberg, R. Macromolecules 2001, 34, 4927–4936.
48. Kuhn, W.; Majer, H. Makromol Chem 1955, 18/19, 239–253.
49. Wedemeyer, W. J.; Xu, X. B.; Welker, E.; Scheraga, H. A. Biochemistry 2002, 41, 1483–1491.
50. Ueberreiter, K.; Kanig, G. J Chem Phys 1950, 18, 399–406.
51. Glans, J. H.; Turner, D. T. Polymer 1981, 22, 1540–1543.

52. Nielsen, L. E. J Macromol Sci Rev Macromol Chem Phys 1969, 3, 69.
53. Tuteja, A.; Mackay, M. E.; Hawker, C. J.; Horn, B. V. Macromolecules 2005, 38, 8000–8011.
54. Mackay, M. E.; Henson, D. J. J Rheol 1998, 42, 1505–1517.
55. Krishnan, R. S.; Mackay, M. E.; Hawker, C. J.; Van Horn, B. Langmuir 2005, 21, 5770–5776.
56. Dee, G. T.; Sauer, B. B. Adv Phys 1998, 47, 161–205.
57. Lomellini, P. Polymer 1992, 33, 1255–1260.
58. Russel, W. B.; Saville, D. A.; Schowalter, W. R. Colloidal Dispersions; Cambridge University Press: Cambridge, 1989.
59. Shah, S. A.; Chen, Y. L.; Schweizer, K. S.; Zukoski, C. F. J Chem Phys 2003, 119, 8747–8760.
60. O'Hern, C. S.; Silbert, L. E.; Liu, A. J.; Nagel, S. R. Phys Rev E: Stat Phys Plasmas Fluids Phys Relat Interdiscip Top 2003, 68, 011306-1–011306-19.
61. Schweizer, K. S. J Chem Phys 1989, 91, 5822–5839.
62. Schweizer, K. S. J Non-Cryst Solids 1991, 131, 643–649.
63. Zimm, B. H. J Chem Phys 1948, 16, 1099–1116.